Supplementary Information

Agrobacteria reprogram virulence gene expression by controlled release of host conjugated signals

Chao Wang[1,3,5,#], Fuzhou Ye[2,#], Changqing Chang[1,#], Xiaoling Liu[2,4], Jianhe Wang[1] Jinpei Wang[1]，Xin-Fu Yan[2], Qinqin Fu[2], Jiannuan Zhou[1], Shaohua Chen[1], Yong-Gui Gao[2,3,*], Lian-Hui Zhang[1,3,*]

Content:

www.pnas.org/cgi/doi/10.1073/pnas.1903695116

Table S1 Bacterial strains and plasmids used in this study

Strain or plasmid	Relevant characteristics	Source or reference
A. tumefaciens		
A6	The wild type octopine strain of *A. tumefaciens*	A. Kerr
SghR:: *Tn5*	A6 carrying a Tn*5* insertion within *SghR*	This study
SghRA:: Tn	SghR::Tn5 carrying a *Mariner* transposition in *sghA*	This study
SghRA::Tn(sghA)	SghRA::Tn carrying pLA-*sghA*	This study
ΔSghA	The wild type of *A. tumefaciens* with SghA deletion	This study
ΔSghR	The wild type of A. tumefaciens with SghR deletion	This study
ΔSghAR	The wild type of A. tumefaciens with double deletion of SghR and SghA	This study
E. coli		
DH5α (λpir)	*supE44 ΔlacU169(Φ80lacZΔM15) hsdR17 recA1 endA1 gyrA96 thi-1 relA1,* λpir	Laboratory collection
BL21(DE3)	*F⁻ ompT hsdS(rB⁻ mB⁻) dcm⁺ Tet^r gal (DE3) endA*	Novagen
BW020767(pRL27)	carrying Tn*5* for *A. tumefaciens* mutagenesis, Kan^r	(1)
SM10(pBT20)	harbouring *Mariner* transposon for *A. tumefaciens* mutagenesis, Get^r	(2)
Acinetobacter sp. ADPWH_lux	*Acinetobacter* sp. containing a *salAR*::*luxCDABE* gene fusion for salicylic acid detection, Amp^r	(3)
Plasmids		
pLA-*sghA*	The broad host range cosmid pLAR3 carrying *sghA* from A6 for complementation analysis, Tc^r,	This study
pQE-*attJ*	pQE3 vector harboring the encoding region of *attJ* from A6, Amp^r	(4)
pET14b-*sghR*	pET14b vector harboring the encoding region of *sghR* from A6, Amp^r	This study
pET14b-*sghA*	pET14b vector harboring the encoding region of *sghA* from A6, Amp^r	This study

Table S2 Primers used in this study

Applications	Primers	Sequence (5'-3')
Construction of pLA-sghA		
	pL3A-F	CGGGATCCGATCTGGTAGGTGTCGTG
	pL3A-R	CAGCCTTTCCACCCTCATCC
RT-PCR of sghA		
	RTA-F	GGCGACCGGCTGGATG
	RTA-R	CGGGGCTTGTTTGGTGG
Real time RT-PCR of sghA		
	qRTA-F	GTGCACGTGGATTACGAAAC
	qRTA-R	CTTCATCACACCGTGATTCC
RT-PCR of sghR		
	RTR-F	CCGTGTCGCGTGCGC
	RTR-R	TGCGTCGTCGCCAGG
Real time RT-PCR of sghR		
	qRTR-F	ACATCGGCGCGGAAACCAAG
	qRTR-R	GAATCCTTGGCGTGGGTGTGAG
RT-PCR of 16s rRNA		
	16S-F	GTGAAATCCCAGAGCTCAACTC
	16S-R	AGTGCAATCCGAACTGAGATG
Real time RT-PCR of rpoC		
	qRTC-F	GGTGACACCGAAGCCTTG
	qRTC-R	GGGTGATGAGACCGTCGTTA
RT-PCR of virA		
	virA-F	AAAGATTGGAGCGCAAGTGT
	virA-R	GAGAAACCATCTCGCGTAGC
Real time RT-PCR of virA		
	qvirA-F	ATATTGGCCCTTATCGTTGC
	qvirA-R	TCGTAGTTGGCTGAGGATTG
RT-PCR of virD2		
	virD-F	GTCACGGCATAGTCCTGGAT
	virD-R	ACATTTGCCTCGGAATCAAC
Real time RT-PCR of virD2		
	qvirD-F	GGAATAGCAGAGCGACCAAT
	qvirD-R	TCGAACGATTGACTGAGGTC

RT-PCR of virE3		
	virE-F	CGTGAGCACGGTAGACTTCG
	virE-R	GAGTTCGTTGCCCTCCTTG
Real time RT-PCR of virE3		
	qvirE-F	GCTCTATCGCGATCTAACCC
	qvirE-R	GTCTGGGAGGTTTGACGATT
Amplification of P*sghA*		
	Bio-sghA-F	Biotin-GCGTGGTTCTGGCAAAC
	Bio-sghA-R	Biotin-GCGCTTTGTGATCGGTC
Amplification of P*pa0305*		
	Bio-p0305-F	Biotin- CTGCTTGGCATGGAGGTACCAGG
	Bio-p0305-R	Biotin- GTTGTCATGCACCAGGCGGCC

Table S3 Summary of crystallographic data and refinement statistics

	Apo	SAG	Salicin	Glucose
Data collection	6RJK	6RK2	6RJO	6RJM
Space group	$P2_12_12_1$	$P2_12_12_1$	$P2_12_12_1$	$P2_12_12_1$
Unit cell dimensions				
a,b,c (Å)	64.2, 80.4, 184.62	63.6, 80.4, 183.6	63.7, 81.0, 183.7	59.0, 84.6, 184.7
α,β,γ (°)	90	90	90	90
Resolution (Å)	50-1.9 (2.1-1.9)	50-2.1 (2.21-2.1)	50-1.8 (1.91-1.8)	50-2.1 (2.24-2.1)
R_{sym} (%)	10.0 (47.1)	9.3 (53.8)	7.0 (60.8)	6.9 (57.2)
I/σI	8.8 (2.5)	10.3 (2.4)	12.1 (1.9)	13.1 (2.2)
Completeness (%)	99.7 (100)	99.2 (98.1)	97.3 (96.8)	98.6 (97.3)
Redundancy	3.4 (3.4)	3.3 (3.4)	3.0 (2.9)	3.3 (3.3)
Refinement				
Resolution (Å)	50-1.9	50-2.1	50-1.8	50-2.1
No. of reflections	73326	104529	152164	98364
R_{work}/R_{free} (%)	17.2/21.8	17.4/21.4	17.3/20.9	18.1/23.0
Average B factor (Å^2)				
Protein	19.9	17.8	17.6	20.7
Ligand	/	25.7	29.7	18.8
Water	27.6	21.2	25.5	22.6
R.m.s.deviations				
Bond length (Å)	0.008	0.008	0.007	0.008
Bond angle (°)	1.09	1.12	1.08	1.08
Ramachandran plot				
Favored regions (%)	97.44	97.11	97.55	96.91
Allowed regions (%)	2.56	2.89	2.45	3.09

* Numbers in parenthesis refer to outer resolution shell

Fig. S1

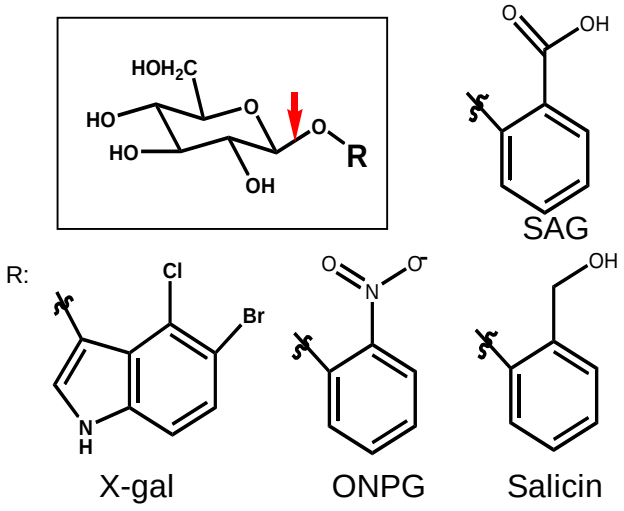

Fig. S1. The similar chemical structures of the compounds used in this study. These compounds contain a common β-D-sugar group and an aromatic ring linked by a glucosidic bond. The common glucose moiety is boxed and the arrow indicates the glucosidic bond on which SghA acts.

Fig. S2

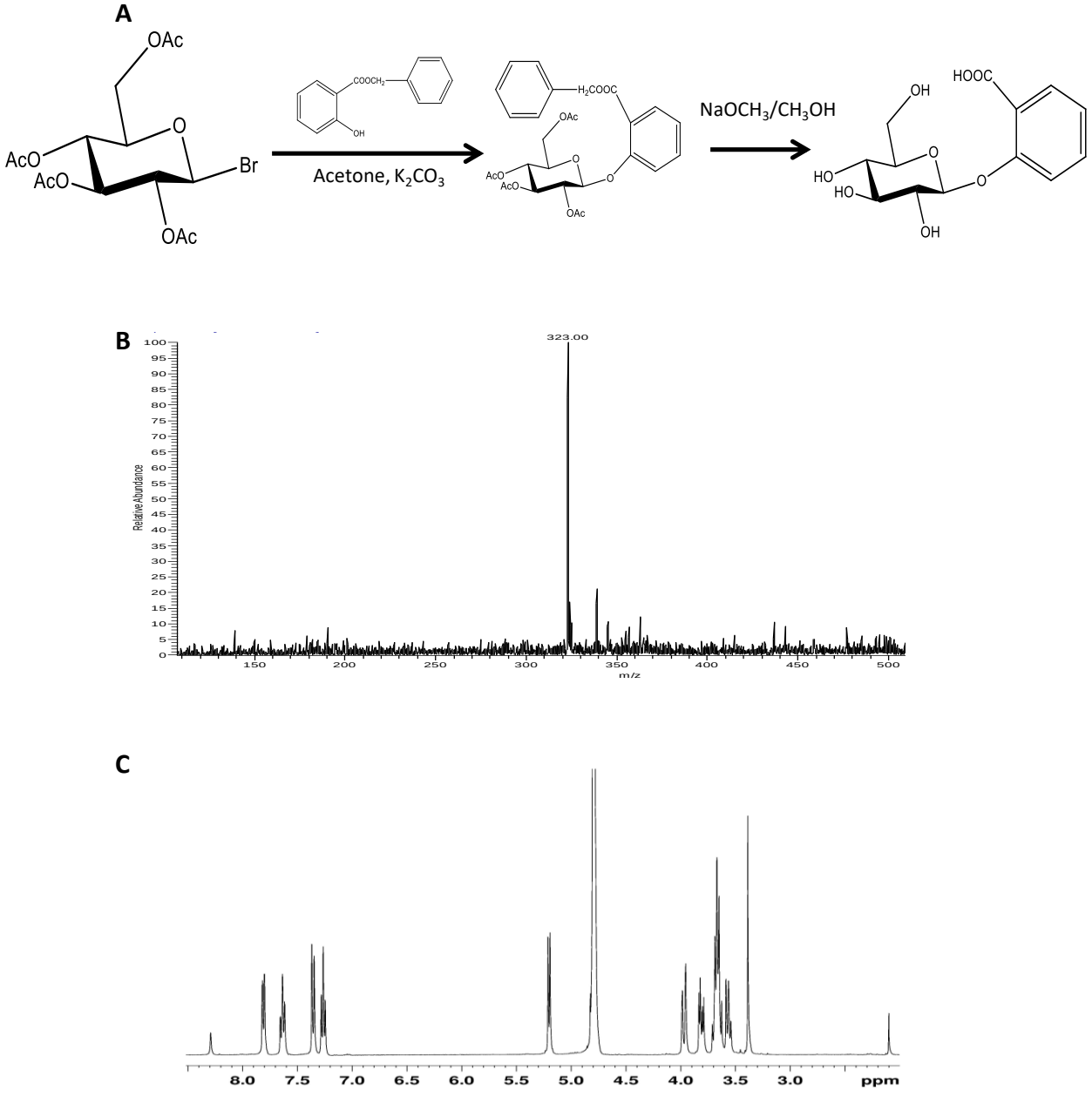

Fig. S2. Chemical synthesis of SAG. A) Schematic representation of SAG synthesis. B) The mass analysis of the synthetic SAG. C) The ^{1}H NMR spectra of the synthetic SAG.

Fig. S3

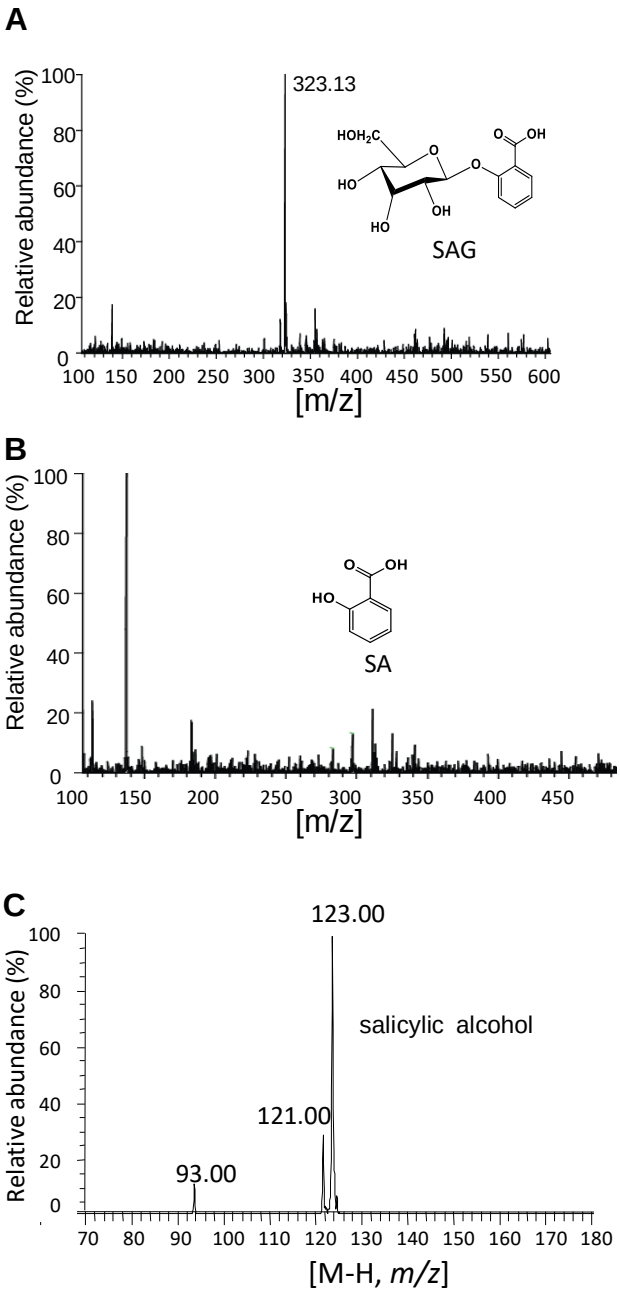

Fig. S3. Characterization of SghA-digested products. A) ESI-MS analysis of the fraction collected at 5.0 min in Fig. 2A. The chemical structure of SAG is shown in inset. B) ESI-MS analysis of the fraction collected at 9.0 min in Fig. 2A. The chemical structure of SA is shown in inlet. C) ESI-MS analysis of the fraction collected at 4.0 min in Fig. 2B.

Fig. S4

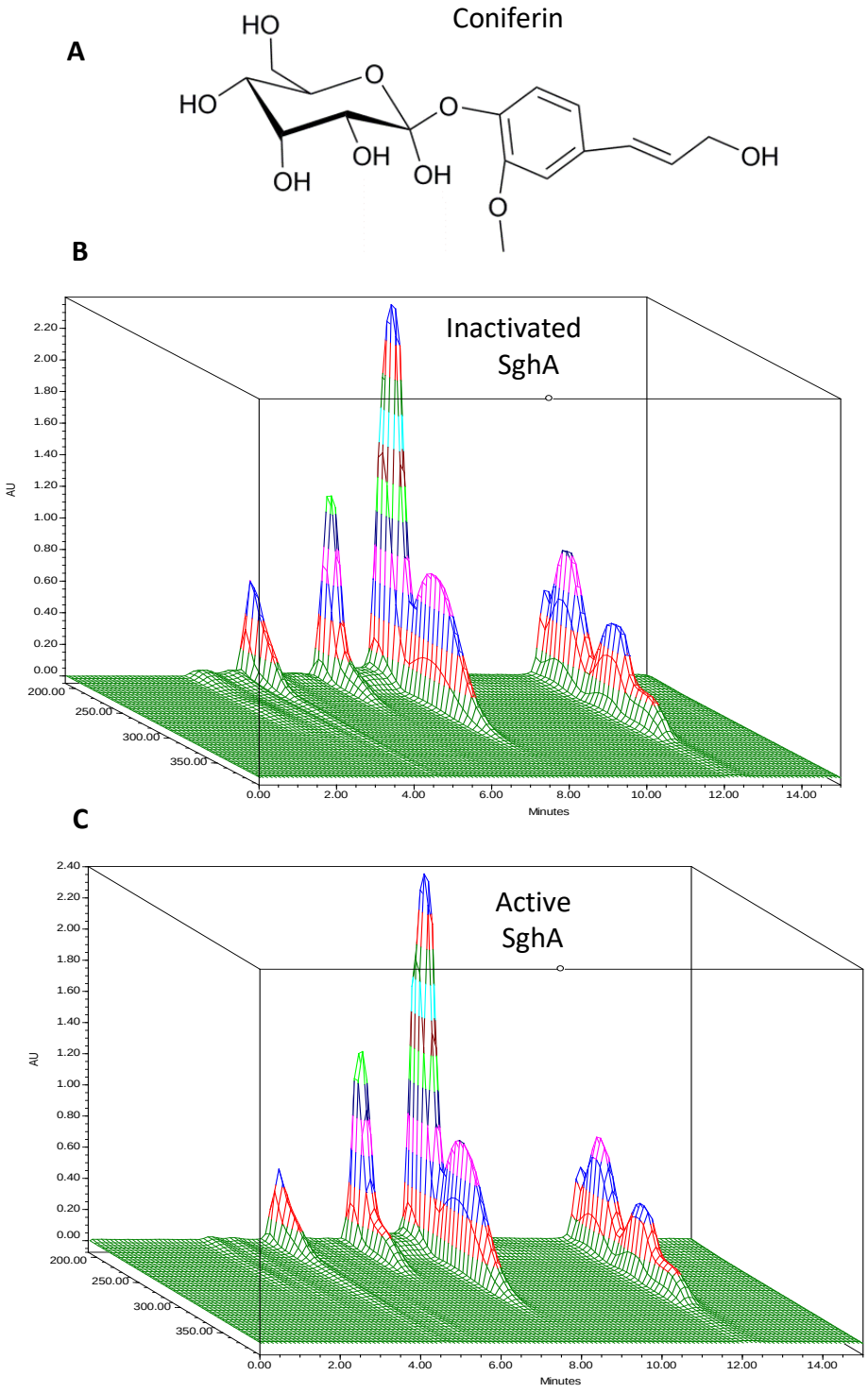

Fig. S4 (A-C). SghA cannot hydrolyze coniferin, the structural analogue of SAG. A) Chemical structure of confierin. B) HPLC profile of reaction mixtures using coniferin as the substrate treated with denatured SghA. C) HPLC profile of reaction mixtures using coniferin as substrate treated with active SghA.

Fig. S4

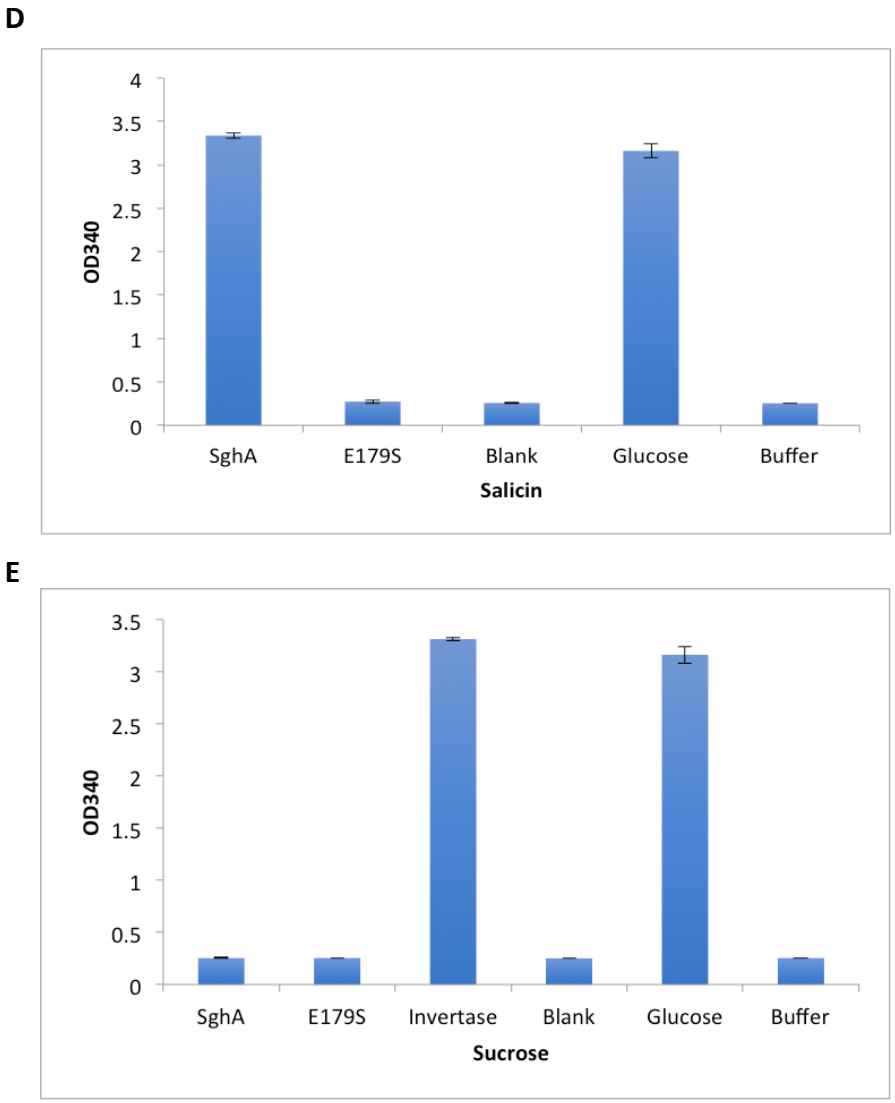

Fig. S4 (D-E). SghA cannot hydrolyze sucrose, the inducer of SghA expression. D) Salicin was used as positive control to verify the enzymatic activity of purified SghA and the validity of biochemical assay. E) Sucrose cannot be hydrolyzed by SghA. Sucrose, Glucose, Salicin, Invertase and Sucrose Assay Reagent were purchased from Sigma, and the reaction product of glucose was detected using Sucrose Assay Kit (Sigma, Cat#: SCA20-1KT). Briefly, 10 mM sucrose (or salicin) were incubated with 160 µg SghA (or its hydrolyase-dead mutant E179S or 2 units of Invertase or buffer) in total volume of 50 µl at 30 ºC for 30 min, and then 50 µl of the Sucrose Assay Reagent to each tube. After an incubation for 15 minutes at room temperature, the .absorbance at 340 nm were measured, respectively.

Fig. S5

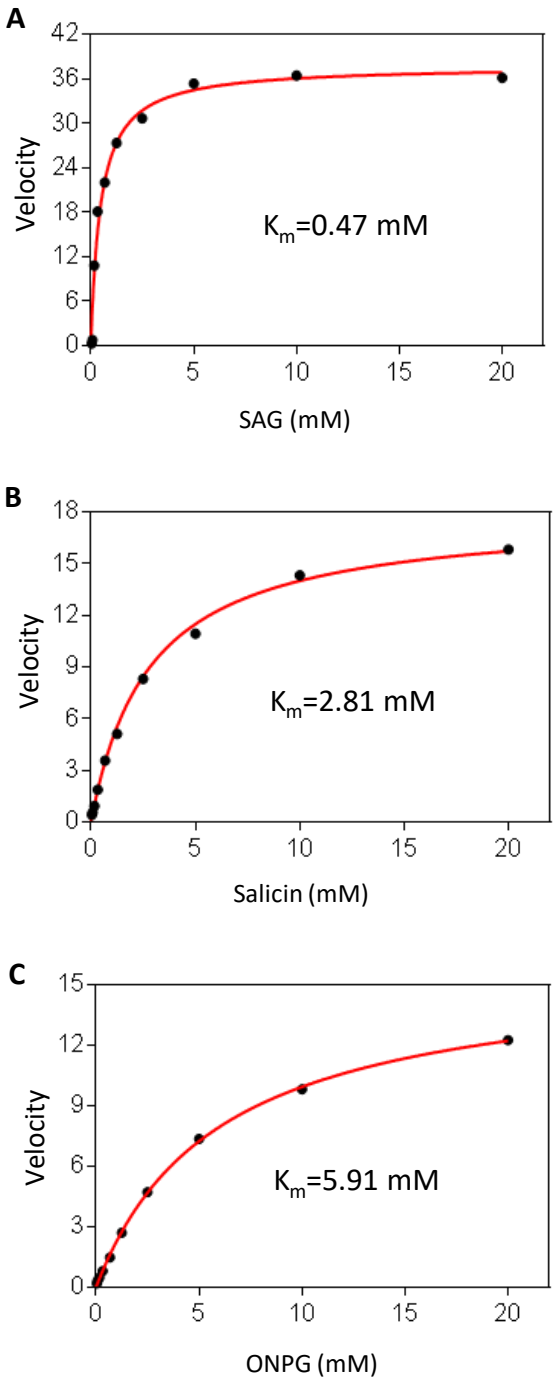

Fig. S5. SghA preferentially hydrolyzes SAG compared with its analogues salicin and ONPG. The Michaelis constant (K_m) of SghA was determined for SAG (A), salicin (B) and ONPG (C) as substrate, respectively.

Fig. S6

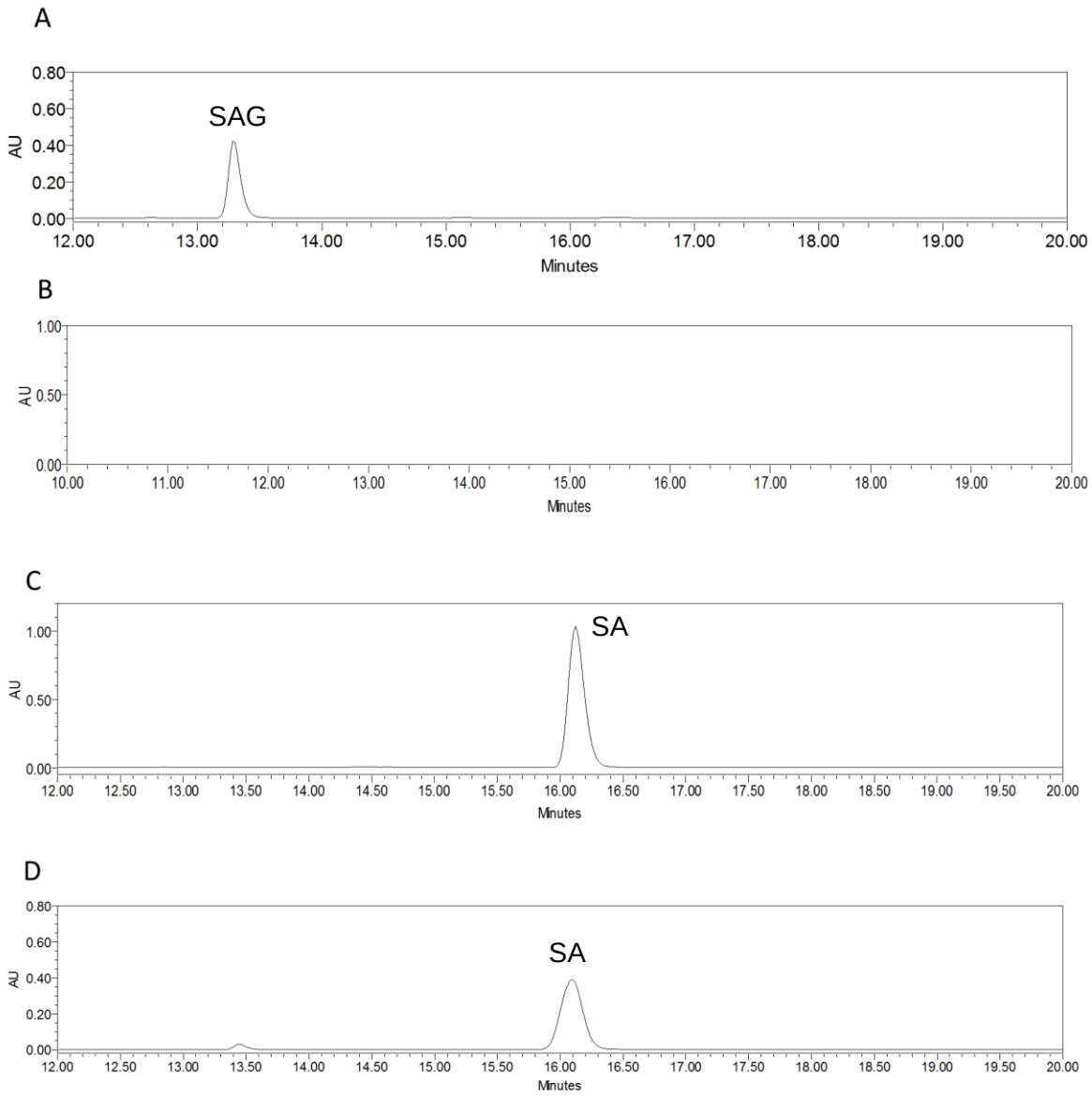

Fig. S6. Degradation of exogenously added SAG by *A. tumefaciens*. (A) HPLC profiles of SAG (8 mM) in BM medium. (B) HPLC profile of the supernatants of bacterial culture growing in BM medium without SAG. (C) HPLC profile of SA (8 mM) in BM medium. (D) HPLC profile of the supernatants of bacterial culture growing in BM medium with SAG. The sghR::Tn5 strain was inoculated in BM medium supplemented with 8 mM SAG at 30 degrees for 1 hours, and then was centrifuged by 14000 rpm for 10 min, the supernatant was extracted by chloroform, subject to freeze dry and resuspended in water for HPLC analysis. The extracted product was subjected to HPLC on C18 reverse column, eluted with gradient acetonitrile –water (0-5 min: 5% acetonitrile; 5-20 min: 5-35% acetonitrile; 20-25 min: 35-95% acetonitrile; 25-30 min: 95-5% acetonitrile) at a flow of 1 ml min^{-1}. The signal was detected by OD_{254}, where SAG was eluted at 13.4 min and SA at 16.2 min. The experiment was repeated twice with similar results.

Fig. S7

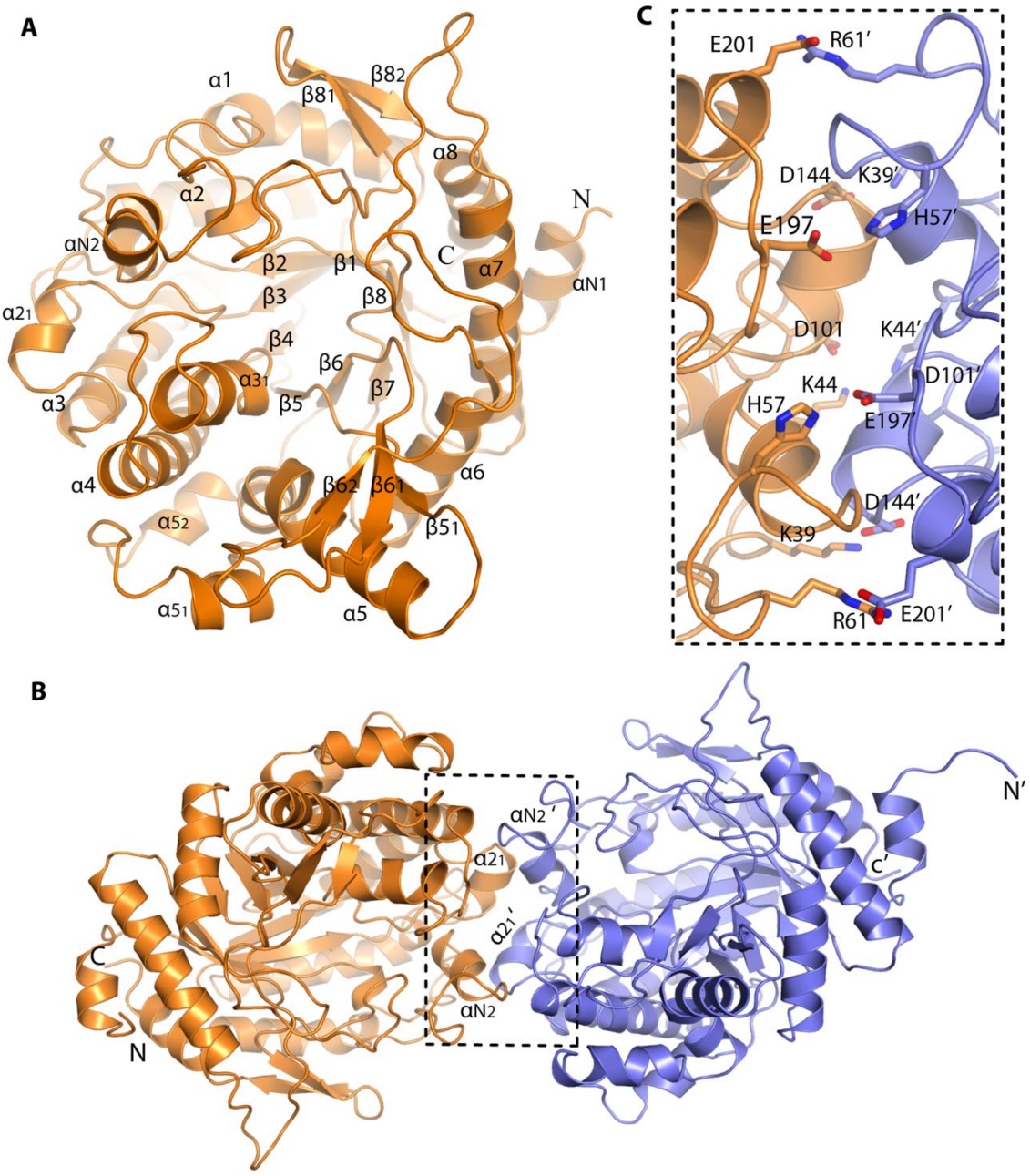

Fig. S7. Overall structure of SghA and its dimerization interface. A) Topology of SghA monomer. B) The structure of SghA dimer. In one homodimer, one monomer is colored light orange and the second monomer colored slate (where primes referred to the second monomer, same as below). The dimerization interface of SghA is boxed with dashed line. C) Enlarged view of the detailed interactions along the dimer interface. Dimer interface residues of SghA were shown as sticks, with oxygen and nitrogen atoms are shown as red and blue respectively.

Fig. S8

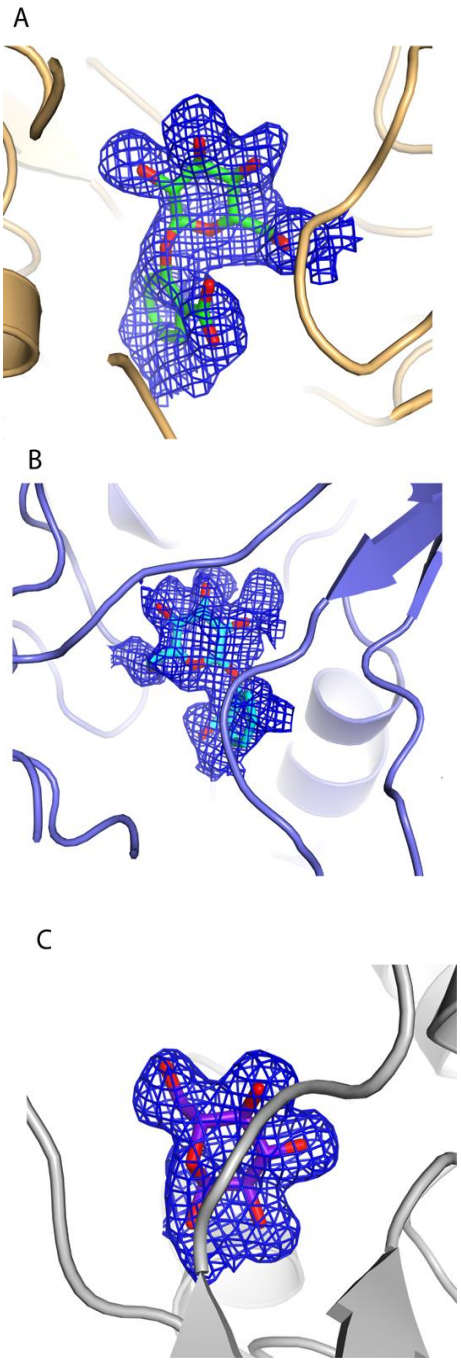

Fig. S8. Unbiased difference Fourier electron density map (Fo-Fc) of SghA with different ligands. SAG, colored green (A), salicin, colored cyan (B), and glucose, colored purple-blue (C).

Fig. S9

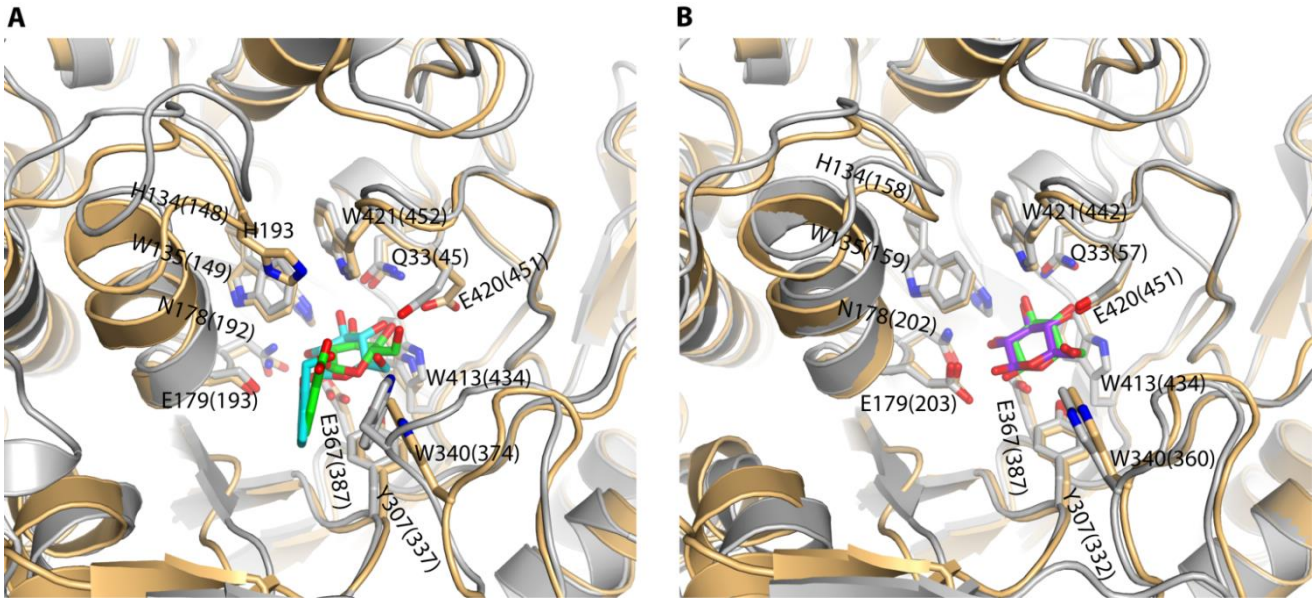

Fig. S9. Structural comparison of SghA with other β-glucosidases. A) Comparison the binding site of SghA-SAG with NkBgl-salicin (PDB code 3VIL). NkBgl (β-glucosidase from *Neotermes koshunensis*) and salicin are colored grey and cyan, respectively. SghA-SAG is represented the same as in Fig. 2C. The residues involving the binding pocket are shown as sticks. The residue outside the bracket, for example W413 of W413(434), indicates the residue from SghA, whereas the residue inside the bracket, W434, from NkBgl. B) Superposition of SghA-glucose with BglB-glucose (PDB code 3FJ0). BglB (β-glucosidase from uncultured soil metagenome) and the product are colored grey and purple-blue, respectively. The structure of SghA (colored light orange) in complex with its reaction product glucose (colored green), in which the active site was found to be almost identical to that of apo form. Structural comparison of SghA-SAG and SghA-glucose shows dramatic conformation change for the side chain of E420, which causes sugar in SAG to be oriented slightly deep inside the binding pocket. As a result, Y307 in SghA establishes hydrogen-bonding interaction with O5 in glucose. Despite this, sugar-binding sites in both structures are quite similar, which is not surprising given a common pattern in sugar recognition by GH1 family enzymes.

Fig. S10

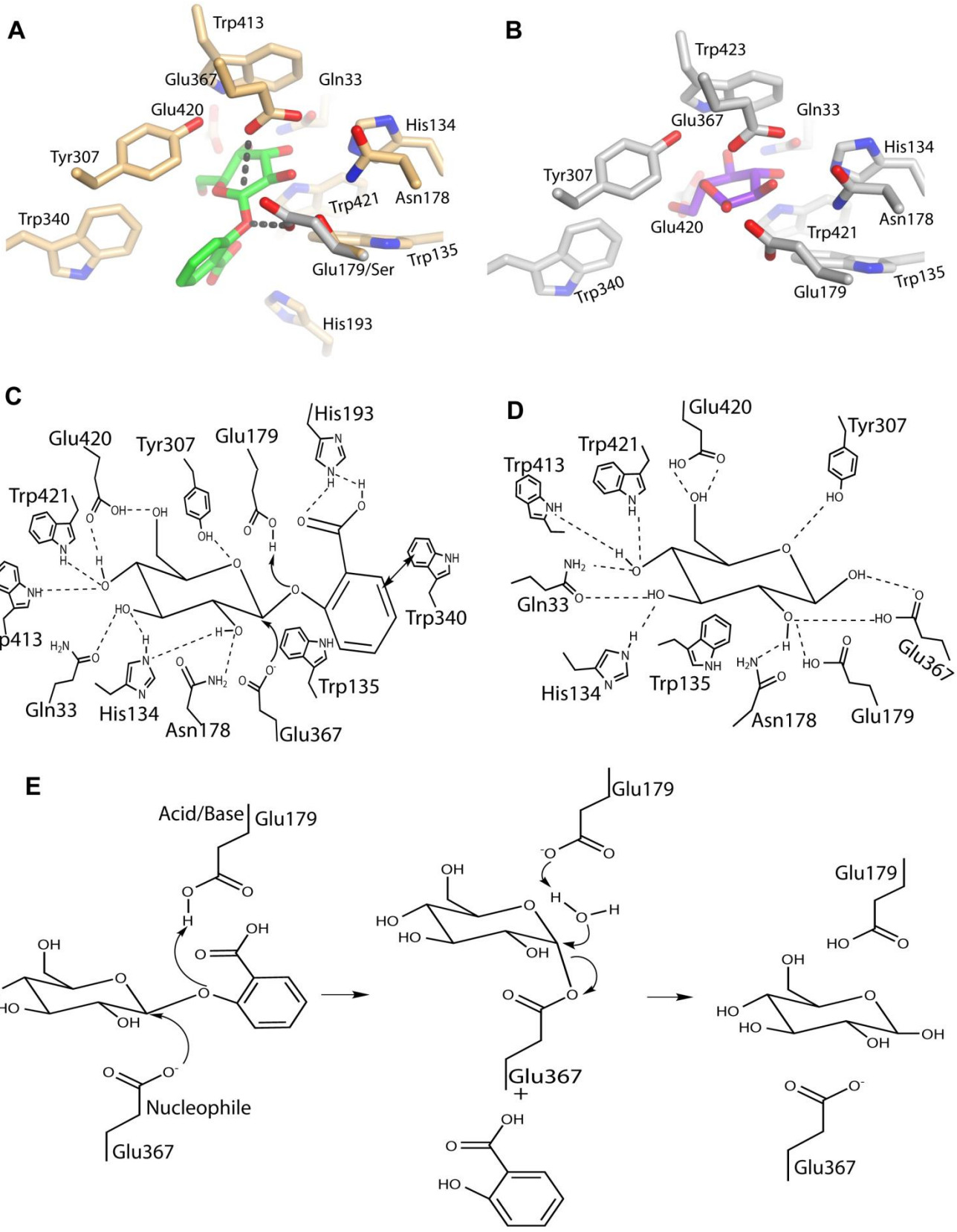
A
Trp413
Glu367
Gln33
Glu420
His134
Tyr307
Trp421
Asn178
Trp340
Glu179/Ser
Trp135
His193
B
Trp423
Glu367
Gln33
Tyr307
His134
Glu420
Asn178
Trp421
Trp340
Glu179
Trp135
C
His193
Glu420
Tyr307
Glu179
Trp421
Trp340
Trp413
Gln33
His134
Asn178
Glu367
Trp135
D
Glu420
Tyr307
Trp421
Trp413
Gln33
His134
Trp135
Asn178
Glu179
Glu367
E
Acid/Base
Glu179
Nucleophile
Glu367
Glu179
Glu367
Glu179
Glu367

Fig. S10. Catalytic mechanism of SghA. The binding pocket of SghA with the substrate SAG (A) and the product glucose (B) presented with SghA colored light orange and grey, and SAG and glucose are shown as green and purple-blue, respectively. The residues involved in SAG/glucose binding were depicted as sticks. (C) and (D) show the detailed interactions of SghA with SAG and glucose, respectively. Hydrogen bonds between SghA and SAG are depicted as dashed lines, and π- π stacking of Trp363 shown as double-ended arrow. E) Schematic representation of the catalytic mechanism of SghA to its substrate SAG. The GH1 family proteins hydrolyze glycosidic bonds through a retention mechanism, which results in an overall retaining of the anomeric configuration of the saccharide substrate. The catalysis involves one highly conserved pair of carboxylic acids, located in motifs T(F/L/M)NE(P/L/I) and (I/V)TENG, that act as an electrophile and a nucleophile, respectively. As expected, our mutation results demonstrated that Glu179 in the motif 176-TFNEP-180, and Glu367 in the motif 365-ITENG-369 are required for the activity. Together with our structures, we proposed a catalytic mechanism of SghA on its substrate SAG. Given the conservation of the active site, superposition of SghA-SAG with SghA-glucose would place Glu179 into its catalytic position, as shown in Fig. S9A and S9B, consequently, both Glu367 and Glu179 are within hydrogen-bonding distance to the anomeric carbon (C1) and glycosidic oxygen (O1). The orientation of SAG for the optimal activity of SghA involves these residues, Gln33, His134, Trp135, Asn178, Glu179, His193, Tyr307, Trp340, Glu367, Trp413, and Glu420, depicted in Fig. 2C and S9A and. In general, Glu367 makes a nucleophilic attack on the anomeric carbon C1, Glu179 acts as a proton donor to release salicylic acid. The resulting glycosyl-SghA, a transition state, was further converted into the final state with product glucose bound via water-mediated hydrolysis, this process involves Glu179 abstracting proton from a water molecule which subsequently acts as the second nucleophilic molecule to attack C1.

Fig. S11

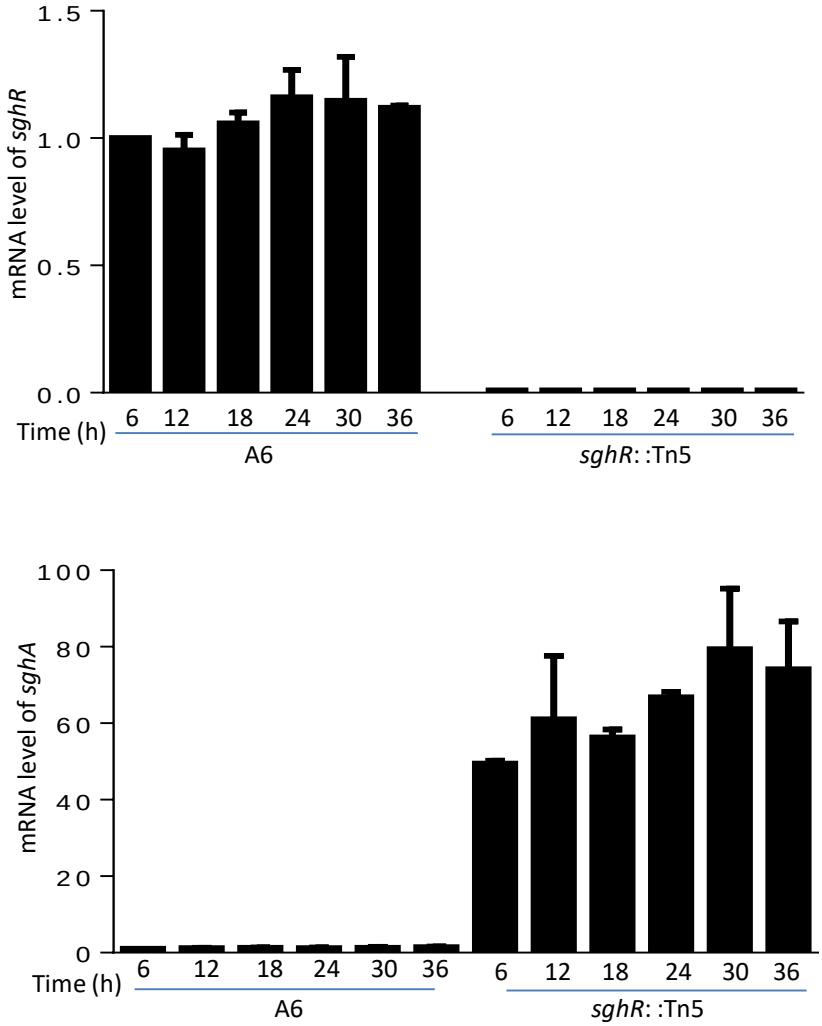

Fig. S11. Quantification of gene expression level by real time RT-PCR. The RNA templates, which were the same as Fig. 3A, were prepared as described in text, and the real time RT-PCR was performed in Rotor-Gene Q (Qiagen) using the primers as described in Table S2. The gene expression level was normalized with the bacterial RNA polymerase subunit gene *rpoC*. For convenience of comparison, the target gene transcript level at 6 h post inoculation was arbitrarily set as 1.

Fig. S12

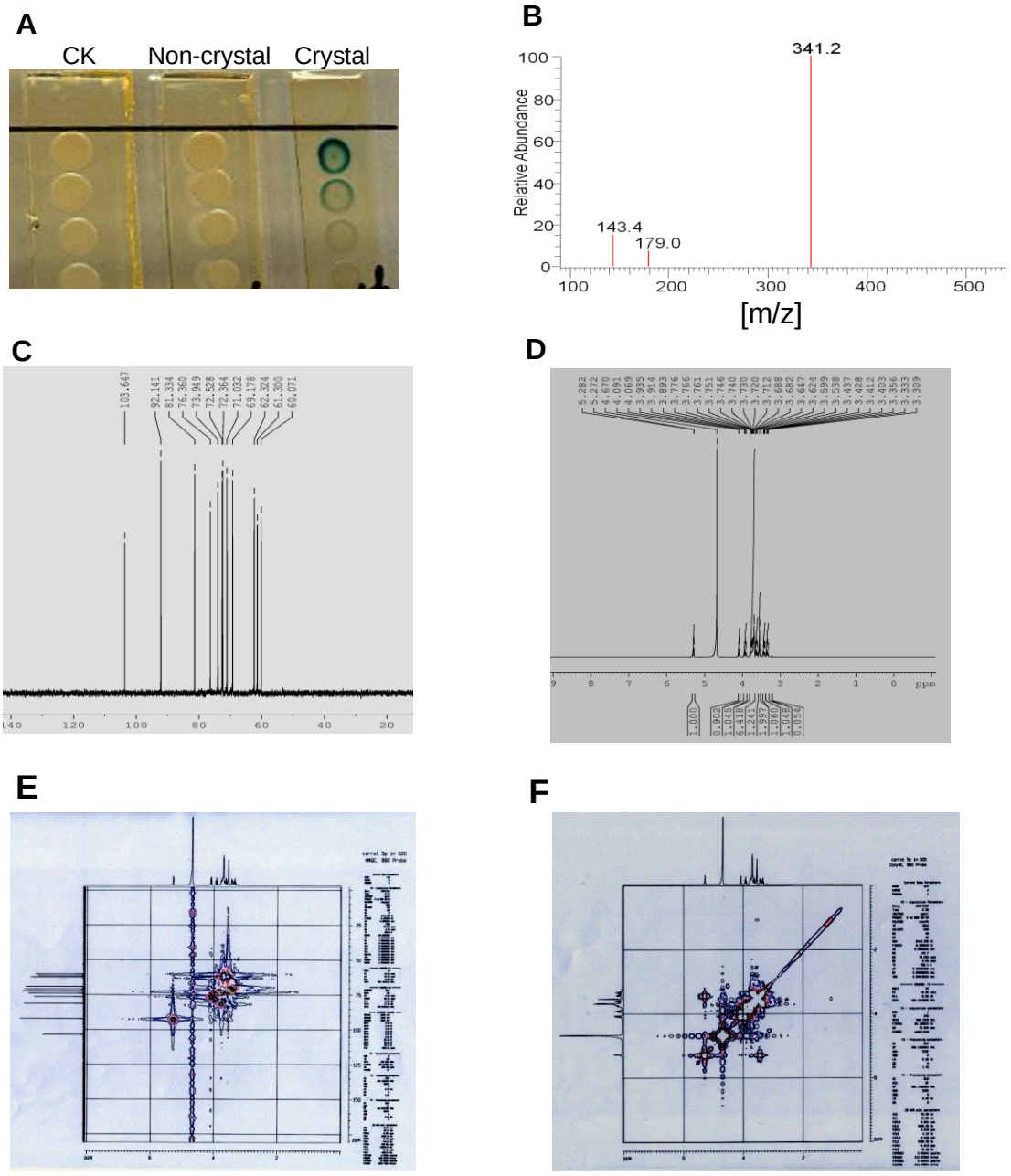

Fig. S12. Identification of sucrose as the plant signal activating the expression of SghA. A) Bioassay of the active crystal after flash column chromatography using the wild type *A. tumefaciens* A6 as the reporter strain. CK: blank control; non-crystal: samples prepared by concentration of the extract after removal the crystal substance; Crystal: solution of the crystalized compound. B) Mass spectrometry analysis of the crystallized compound. C) ^{13}C NMR spectrum of the crystallized compound. D) ^{1}H NMR spectrum of the crystallized compound. E) HMQC analysis of the crystallized compound. F) COSY analysis of the crystallized compound.

Fig. S13

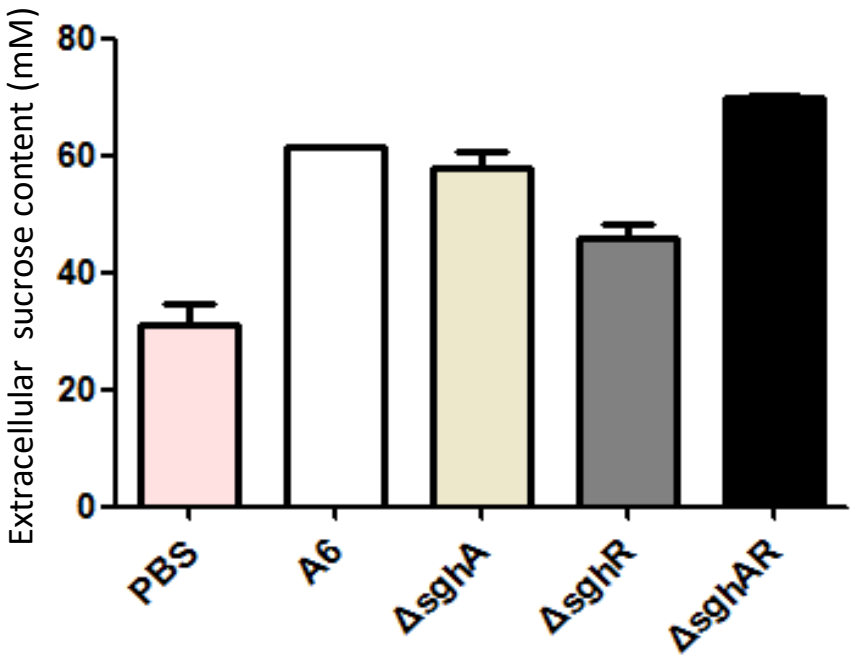

Fig. S13. Sucrose contents in carrot slices at different time points after inoculation with *A. tumefaciens* strain A6 and its derivatives. Bacterial inoculum suspended in PBS buffer, which alone was used as a blank control (CK), was applied onto the surface of carrot slice. The inoculated and CK tissues were kept at 28 °C and apoplastic fluid was collected with the infiltration technique as previously published (5). The sucrose content of apoplast is determined according to the instructions of sucrose assay kit (Sigma).

Fig. S14

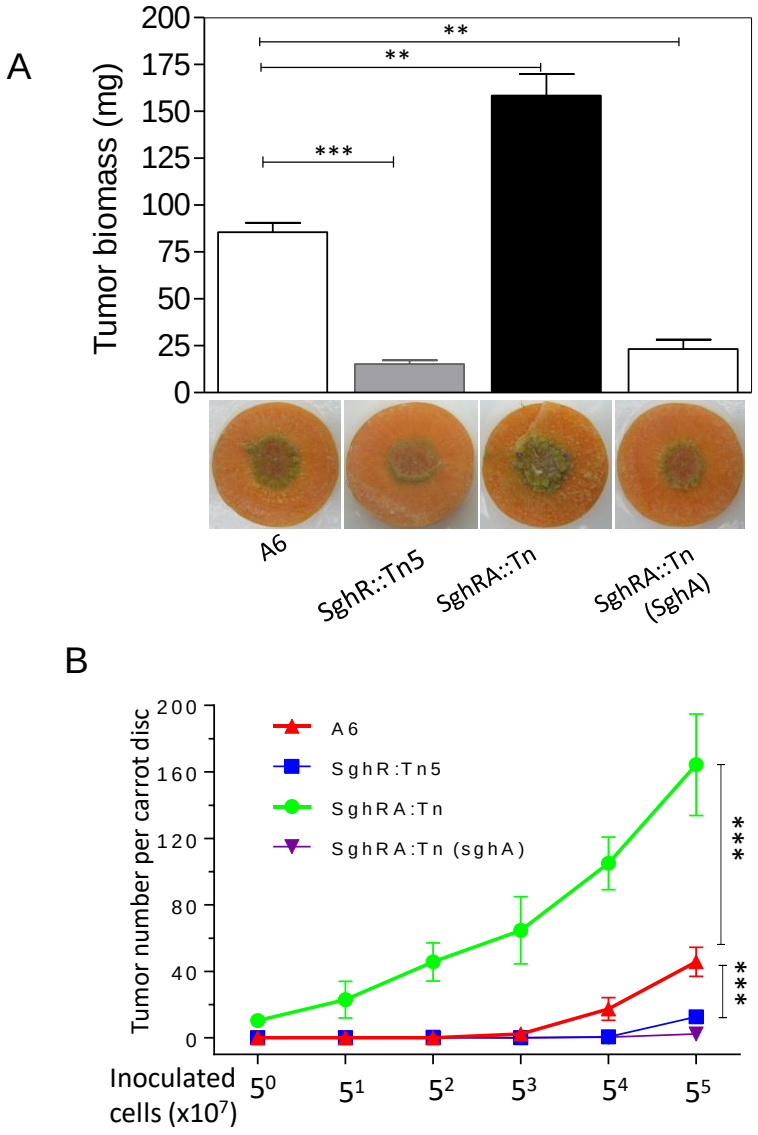

Fig. S14. Tumorigenecity assay for *A. tumefaciens* A6 and its derivatives using carrot discs. (A) Determination of tumor growth in carrot tissues. Representative images (bottom) were taken and fresh weight of tumors (top) were recorded at 4-week after inoculation. (B) Measurement of tumor numbers incited by strain A6 and derivatives. Specified bacterial strains were separately cultured in LB medium. When OD_{600} reached to 1.0, 2 ml of bacterial cultures were centrifuged and the bacterial cells were washed with PBS buffer and resuspended in 1 ml of PBS. Then the bacterial cells were serially diluted by 5 folds, and applied to sterile carrot discs, which were then placed in the petri dishes with filter paper saturated with PBS. After 5-day incubation at 28°C, the number of tumours was recorded under a microscope. Symbol, **: very significant , ***: highly significant, The data shown are one set of representative results from two sets of independent experiments, each with 5 duplicates.

Fig. S15

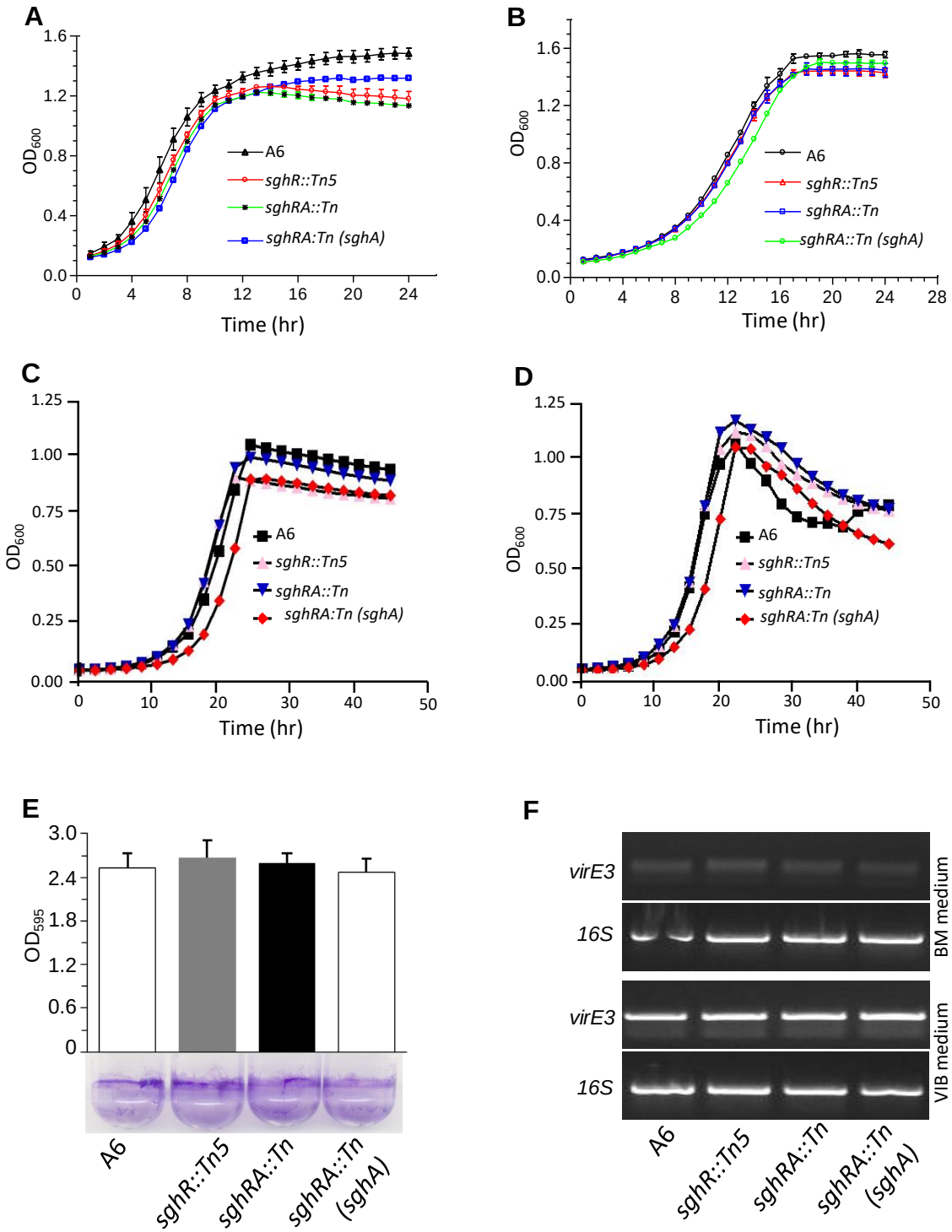
A
B
C
D
E
F
OD600
OD595
Time (hr)
A6
sghR::Tn5
sghRA::Tn
sghRA:Tn (sghA)
sghRA::Tn (sghA)
virE3
16S
BM medium
VIB medium
A6
sghR::Tn5
sghRA::Tn
sghRA::Tn (sghA)

Fig. S15. Analysis of the roles of SghA on *A. tumefaciens* physiology and *vir* gene expression under *in vitro* conditions. A) Bacterial growth curves in LB medium. B) Bacterial growth curves in BM media with mannitol as the sole carbon source. C) Growth curves for the wild type strain A6 and its mutants using glucose as the sole carbon source. D) Growth curves for the wild type strain A6 and its mutants using sucrose as the sole carbon source. E) Quantification (top) and representative image (bottom) of biofilm formation for the wild type strain A6 and its mutants. F) RT-PCR analysis of *virE3* for the mutants of *A. tumefaciens* A6 grown in BM minimal medium in which a low basal expression of virE3 was detected (top) and in VIB medium (bottom)

Fig. S16

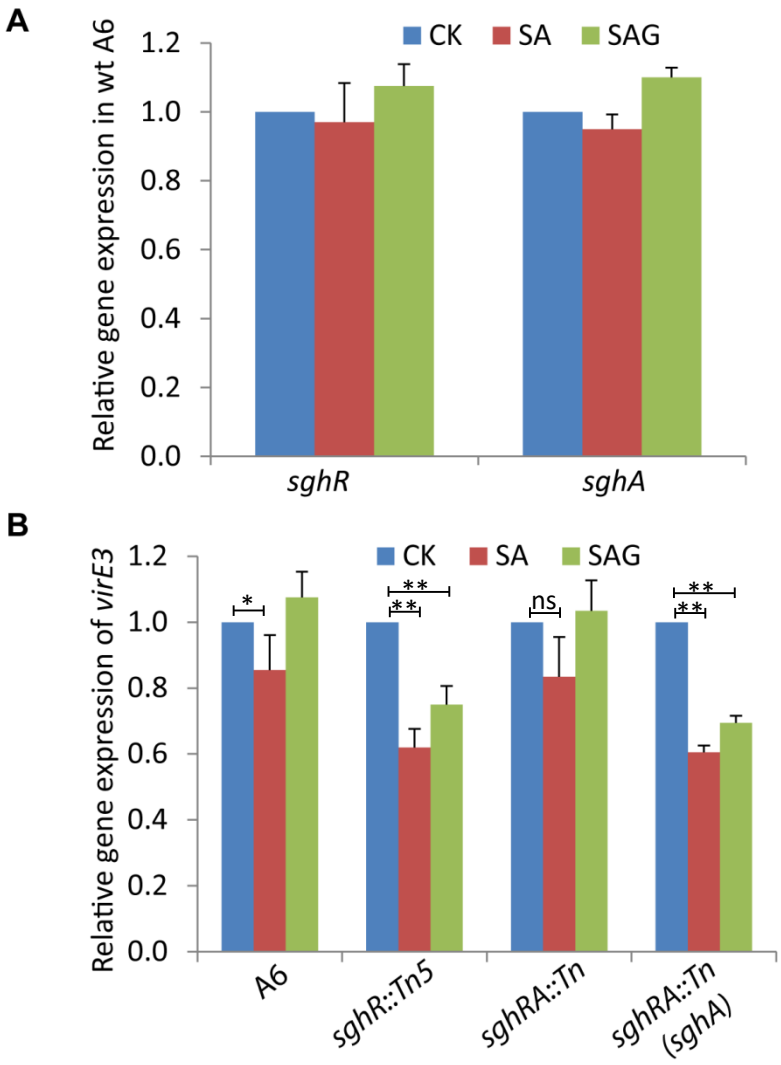

Fig. S16. Effect of SA and SAG on transcriptional expression of *sgh* and *vir* genes of *A. tumefaciens* strains cultured in BM minimal medium. A) SA and SAG have no detectable effects on the expression of *sghR* and *sghA* in the wild type *A. tumefaciens* strain A6. B) SA and SAG inhibited the expression of *virE3*, but the effect of SAG is dependent on the presence of functional SghA. The transcriptional analysis was conducted using real time RT-PCR, and the expression level of blank control (CK) was arbitrarily set as 1. Symbol, *: significant, **: very significant, ns: not significant.

Fig. S17

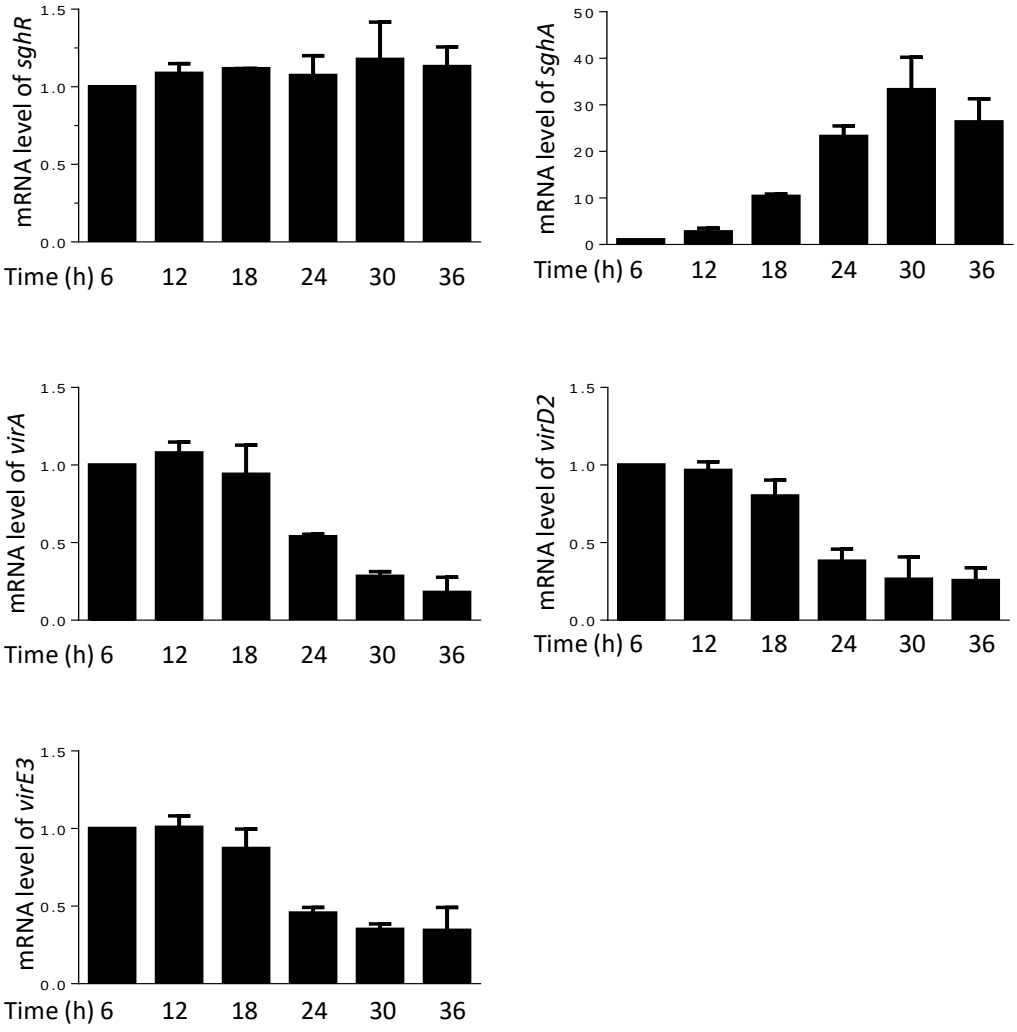

Fig. S17. Quantification of gene expression level by real time RT-PCR analysis. The RNA templates were the same used for Fig. 6B, and the real time RT-PCR was performed in Rotor-Gene Q (Qiagen) using the primers as described in Table S2. The gene expression level was normalized with the bacterial RNA polymerase subunit gene *rpoC*, and the target gene transcript level at 6 h post inoculation was arbitrarily set as 1.

Reference

1. Larsen RA, Wilson MM, Guss AM, & Metcalf WW (2002) Genetic analysis of pigment biosynthesis in Xanthobacter autotrophicus Py2 using a new, highly efficient transposon mutagenesis system that is functional in a wide variety of bacteria. *Arch Microbiol* 178(3):193-201.

2. Kulasekara HD*, et al.* (2005) A novel two-component system controls the expression of Pseudomonas aeruginosa fimbrial cup genes. *Mol Microbiol* 55(2):368-380.

3. Huang WE*, et al.* (2005) Chromosomally located gene fusions constructed in Acinetobacter sp. ADP1 for the detection of salicylate. *Environ Microbiol* 7(9):1339-1348.

4. Zhang HB, Wang LH, & Zhang LH (2002) Genetic control of quorum-sensing signal turnover in Agrobacterium tumefaciens. *Proc Natl Acad Sci U S A* 99(7):4638-4643.

5. David P. Livingston & Henson CA (1998) Apoplastic sugars, fructans, fructan exohydrolase, and Invertase in Winter Oat: responses to second-phase cold hardening. Plant Physiol 116: 405-408